Applied Surface Science 258 (2012) 9816–9823

Contents lists available at SciVerse ScienceDirect

Applied Surface Science

journal homepage: www.elsevier.com/locate/apsusc

Effect of periodic surface cracks on the interfacial fracture of thermal barrier coating system

X.L. Fan [a,b], R. Xu [a], W.X. Zhang [a], T.J. Wang [a,*]

[a] State Key Laboratory for Strength and Vibration of Mechanical Structures, Department of Engineering Mechanics, School of Aerospace Engineering, Xi'an Jiaotong University, Xi'an 710049, China
[b] School of Aeronautics, Northwestern Polytechnical University, Xi'an 710072, China

ARTICLE INFO

Article history:
Received 6 May 2012
Received in revised form 7 June 2012
Accepted 8 June 2012
Available online 17 June 2012

Keywords:
Surface crack
Delamination
Thermal barrier coating
Energy release rate

ABSTRACT

Periodic surface cracks and interfacial debonding in thermal barrier coating (TBC) system may be induced during cooling process. The objective of this work is to investigate the effect of periodic surface cracks on the interfacial fracture of TBC system. The finite element method (FEM) incorporating cohesive zone model is used in analysis. It is found that surface crack spacing has significant effect on the initiation and propagation of short interface crack. Three different regions are identified for describing the effect of surface crack spacing. In Region I the interface crack driving force is dramatically reduced due to high surface crack density. In this case, the initiation of interfacial delamination can be delayed. Region II applies as the surface crack spacing is moderate. Analysis of this transition zone brings to the definition of normalized critical surface crack spacing. Region III arises for sufficient large surface crack spacing. In this case, the interface crack driving force reaches a steady state, where the effects of adjacent surface cracks are relatively insignificant and can be ignored. It can be concluded that an appropriately high surface crack density can enhance the durability of TBC system.

1. Introduction

Multiple surface cracking and/or interface debonding are the major failure mechanisms in materials and film/substrate systems [1–3], e.g. inclusion/matrix in materials, thermal barrier coating (TBC) system, etc., which are important for the strength and safety evaluation of materials and structures. Erdogan [4] analytically studied the problem of periodic surface cracks in nonhomogeneous materials under shear deformation and obtained analytical solutions for the problem. The effects of geometrical and material parameters were analyzed by Schulze and Erdogan [5], Kokini et al. [6], Fan et al. [7] and Zhang et al. [8]. Periodic arrays of cracks in a finite trip under surface heating were investigated by Rizk [9]. The effect of compliant substrate on the periodic surface cracking was studied by Thouless et al. [10], in which a critical toughness ratio of film to substrate was defined to predict the catastrophic failure of substrate. It is assumed in most of these investigations that the film is well bonded to the substrate, and the fact that interface crack may be initiated due to the stress concentration at the channel crack tip is ignored in analysis.

More recently, studies have been focused on the debonding of pre-tensioned films from substrates and the interaction between surface cracks and interfacial delamination. Lu and Erdogan [11] analytically investigated the singular fields near and at the intersection point of an interfacial delamination and a surface crack. Zhou and Kokini [12,13] presented an analytical model and predicted the interfacial fracture mechanism of TBC system with multiple surface cracks. Wu et al. [14] numerically studied the redistribution of interfacial stress due to periodic segmentation cracks in the coating. A failure map for the initiation of interface crack from the root of a channel crack was proposed by Mei et al. [15] to study the effect of interface crack on channel cracking of thin films, in which only one dominate surface crack was considered.

The original motivation of the present study is the authors' experimental observation to TBC system, as shown in Fig. 1, where concomitant interfacial delamination initiates from the roots of almost equally distributed surface cracks. However, most of the previous studies have ignored the interaction of multiple surface cracks and interfacial cracks, and much less attention has been paid directly to the effect of periodic surface cracks on the coating debonding and the durability of TBC system. Although Zhou and Kokini [12] analyzed the effect of surface crack morphology on the interfacial delamination, it was limited to preset and half-way surface cracks instead of channel cracks and the process of initiation and propagation of interface crack was ignored in analysis, which is, however, most important while examining the coating debonding from substrate. The present work aims to investigate the effect of multiple channeling cracks on the formation and propagation

* Corresponding author. Tel.: +86 29 82663318; fax: +86 29 82669044.
E-mail address: wangtj@mail.xjtu.edu.cn (T.J. Wang).

0169-4332/$ – see front matter © 2012 Elsevier B.V. All rights reserved.
http://dx.doi.org/10.1016/j.apsusc.2012.06.036

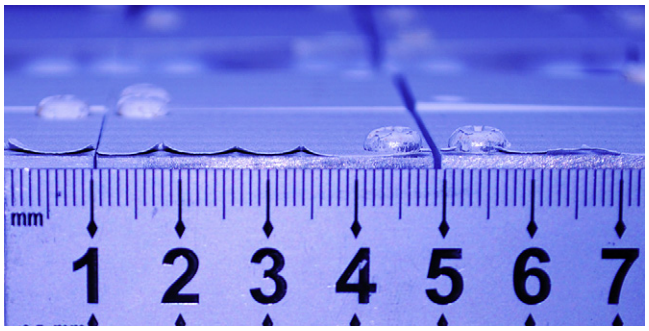

Fig. 1. A photograph shows crack patterns of multiple surface cracks and interfacial debonding.

of interfacial delamination and related interfacial fracture mechanism in TBC system. In Section 2, we firstly descript the problem of multiple surface cracks and interfacial delamination in TBC, and then the numerical model is developed. In Section 3, the crack driving forces for both surface and interfacial cracks are calculated, and moreover the effect of surface cracks on interfacial delamination is discussed in detail. Section 4 summarizes the concluding remarks and emphasizes the positive potential of periodic surface cracks to improve the durability of TBC system.

2. Statement of the problem

Usually, a TBC system comprises a ceramic top coat, a bond coat and a metal substrate. An appreciable temperature difference exists between the heat resistant ceramic top coat and the load bearing alloy substrate. Due to the difference of thermal expansion coefficients of the elements, stresses may be developed upon thermal cycling, which may cause the debonding of top coat from the substrate. In practice, actual spalling failure of TBC is preceded by multiple surface cracks that propagate and coalesce with interfacial crack between the top coat and the bond coat, as shown in Fig. 1. A steady state concept for cracks in multilayer structure is essential for many situations, where the crack driving force of channeling crack is independent of the tunnel length. Once the steady state is reached, the crack driving force can be calculated by using a two-dimensional (2D) plane strain model [16]. Fig. 2 shows the 2D plane strain model of steady state multiple channel cracks accompanied with interfacial cracks, in which h_f, d and W are the film thickness, the deflected interfacial crack length, and the surface crack spacing, respectively.

Based on our experimental observation shown in Fig. 1, the distance between adjacent surface cracks is roughly twenty to thirty times the film thickness. In other words, multiple surface cracks in the film are equally nucleated. Therefore, a unit cell model can be constructed by using periodic boundary conditions. As a result, a three-dimensional periodic surface cracking problem is reduced to a 2D plane stain model, as shown in Fig. 3.

Considering the problem shown in Fig. 3, it was observed that the elastic mismatch of the problem can be expressed in terms of two nondimensional parameters α and β. Under the assumption of plane strain problem, the Dundurs' parameters α and β are expressed as

$$\alpha = \frac{\bar{E}_1 - \bar{E}_2}{\bar{E}_1 + \bar{E}_2} \tag{1}$$

$$\beta = \frac{1}{2}\frac{\mu_1(1-2\nu_2) - \mu_2(1-2\nu_1)}{\mu_1(1-\nu_2) - \mu_2(1-\nu_1)} \tag{2}$$

where $\bar{E}_i = E_i/(1-\nu_i^2)$, E_i, ν_i and μ_i (i = 1, 2) are the plane strain modulus, Young's modulus, Poisson's ratio, and shear modulus of the respective materials, respectively. For most problems, α is more important than β. If material 1 has the same properties as material 2, then $\alpha = \beta = 0$.

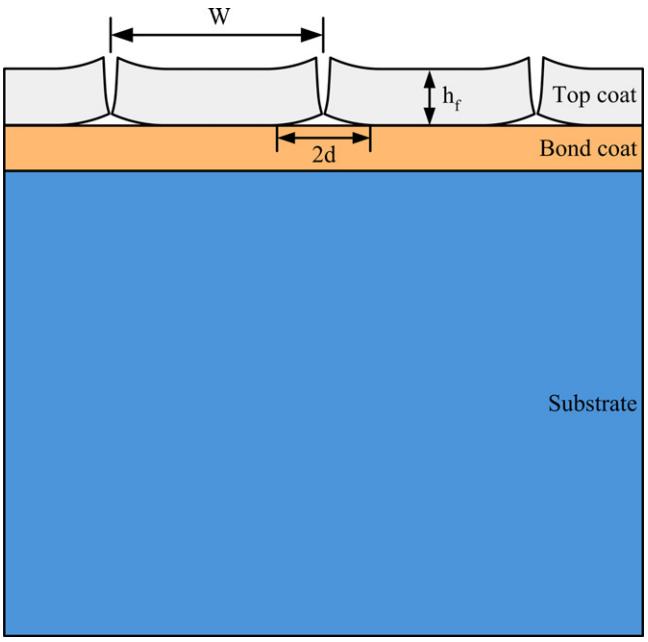

Fig. 2. Schematic illustration of two-dimensional plane strain problem for steady state periodic channeling cracks with interfacial cracks.

The singularity of interface crack tip field can be developed by using the bimaterial constant ε defined as

$$\varepsilon = \frac{1}{2\pi}\ln\frac{1-\beta}{1+\beta} \tag{3}$$

The traction on the interface ahead of the kinked interface crack tip can be written as

$$\sigma_{yy}(x,0) + i\sigma_{xy}(x,0) = (K_1 + iK_2)(2\pi r)^{-1/2} r^{i\varepsilon} \tag{4}$$

where $i = \sqrt{-1}$, $r^{i\varepsilon} = \cos(\varepsilon \ln r) + i\sin(\varepsilon \ln r)$ is the oscillatory singularity parameter for bimaterial interface crack problem.

For a deflected interface crack, an asymptotic solution of the complex interface stress intensity factor (SIF) K is [17]

$$K = K_1 + iK_2 = k_1 d^{1/2-\lambda}[C(\alpha,\beta)d^{i\varepsilon} + D(\alpha,\beta)d^{-i\varepsilon}] \tag{5}$$

where k_1 is a scale factor proportional to external load applied to the cracked body, λ is real and depends on Dundurs' parameters, C and D are dimensionless complex functions of α and β. The detail of the solution procedure for C and D were given by He and Hutchinson [17]. The aforementioned formulas were originally proposed for a

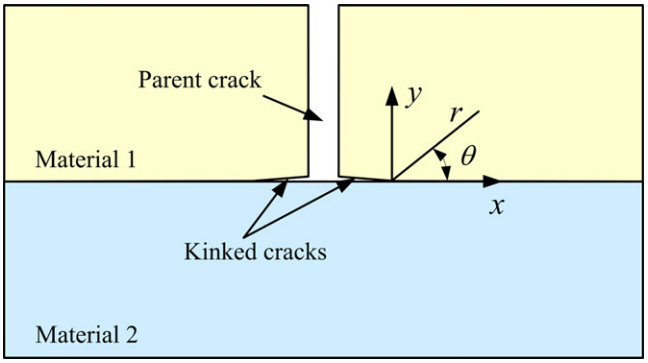

Fig. 3. Geometry and local coordinates of an interface crack initiating from the root of a surface crack.

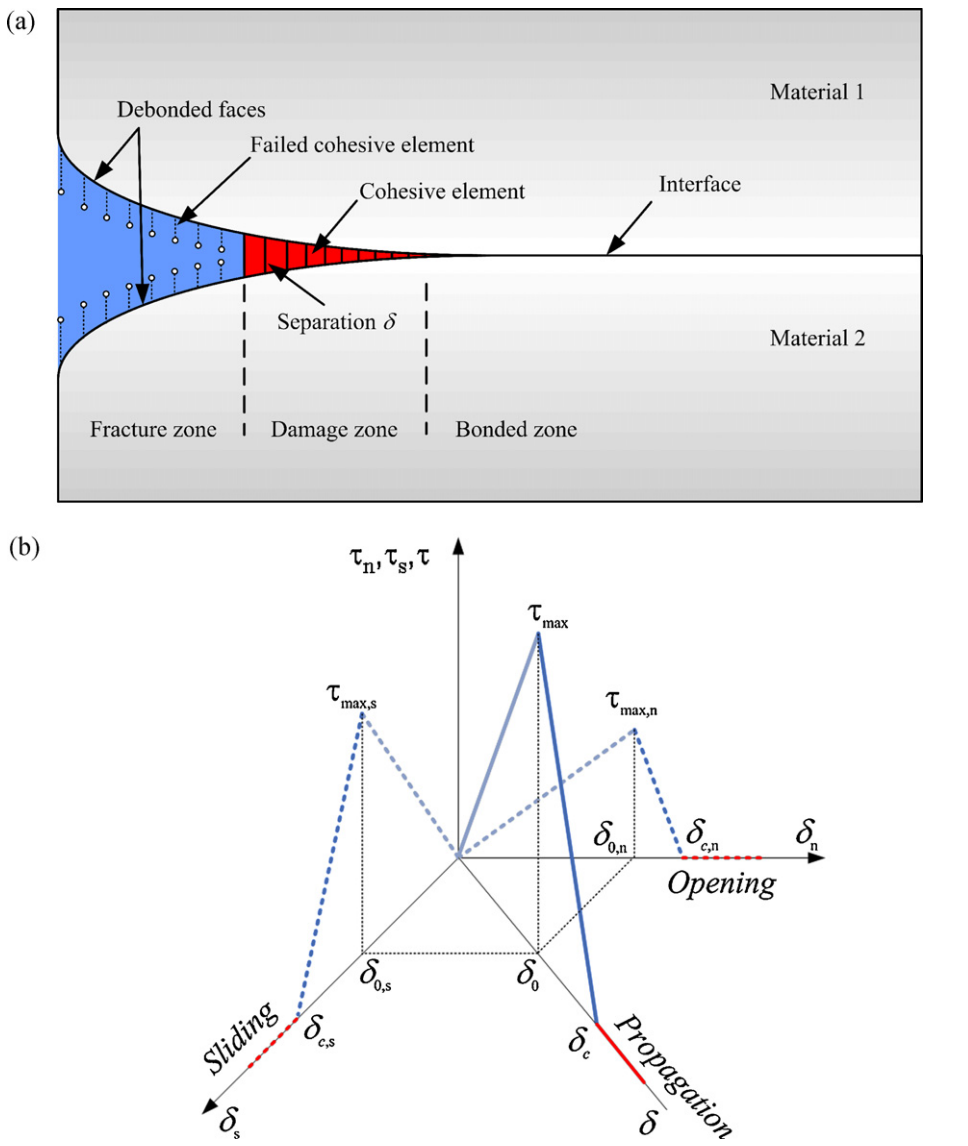

Fig. 4. Schematic presentation of (a) the cohesive zone concept and (b) a mixed mode cohesive law.

bi-layer structure, which are adopted herein to study the fracture behavior of TBC system.

According to Irwin's relation between the strain energy release rate (SERR) and SIF, SERR of the interface crack can be written as [17]

$$G_d = \left(\frac{1}{\bar{E}_1} + \frac{1}{\bar{E}_2}\right)\frac{K_1^2 + K_2^2}{2\cosh^2 \pi\varepsilon}$$

$$= \left(\frac{1}{\bar{E}_1} + \frac{1}{\bar{E}_2}\right)\frac{k_1^2\left[\left|C\right|^2 + 2Re(CD) + \left|D\right|^2\right]}{2\cosh^2 \pi\varepsilon} d^{1-2\lambda} \quad (6)$$

Usually, the interface is a low-toughness fracture path. So, the propagation of interfacial delamination between two different materials is usually a mixed mode fracture problem. Experiments show that the interfacial toughness in this case is not a single material parameter but a function of mode mixity ψ defined by [16]

$$\psi = \tan^{-1}\left(\frac{\sigma_{12}}{\sigma_{22}}\bigg|_{r=l}\right) = \tan^{-1}\left(\frac{Im\, KI^{i\varepsilon}}{Re\, KI^{i\varepsilon}}\right) \quad (7)$$

where l is a reference length. It is seen that ψ is the relative amount of mode 2 to mode 1 at a fixed distance ahead of the crack tip. For the prediction of mixed mode fracture of a bimaterial system, an in-plane length is preferred [16]. The coating thickness h_f is chosen as the reference length herein.

The stress fields and the evolution of crack driving force may become quite complex for an interfacial delamination emanating from the root of surface crack. The finite element method incorporating cohesive zone model (CZM) is therefore adopted to solve the problem. The origin of CZM method goes back to Dugdale [18] and later the cohesive zone concept was embedded into numerical simulation schemes [19]. A cohesive zone is assumed in front of the crack tip along the plane of potential crack propagation, as shown in Fig. 4(a). CZM relates traction to displacement jump at an interface where a crack may initiate or propagate. Damage occurs when the maximum traction τ_{max} is greater than the interfacial strength of the problem. The traction reduces to zero and new crack surfaces formed once the area under the traction–displacement curve is equal to the interfacial fracture toughness G_c or the critical separation δ_c is reached, as shown in Fig. 4(b).

Under mixed mode loading, interface crack initiates as a scalar function of interfacial stresses reaches a limit. The following crack

Table 1
Material parameters of the cohesive elements.

τ_n^0 (MPa)	τ_s^0 (MPa)	G_n^c (J/m^2)	G_s^c (J/m^2)	η
30	30	3	3	1.45

initiation criterion [20] that accounts for the interaction of traction components is adopted in analysis,

$$\left(\frac{\langle\tau_n\rangle}{\tau_n^0}\right)^2+\left(\frac{\tau_s}{\tau_s^0}\right)^2+\left(\frac{\tau_t}{\tau_t^0}\right)^2=1 \tag{8}$$

where $\langle\bullet\rangle$ is the MacAuley bracket defined as $\langle x\rangle = 1/2(x+|x|)$, denoting that the term is set to zero if the quantity enclosed is negative.

Usually, the criterion for damage evolution in CZM is independent of the crack initiation. To accurately account for the variation of fracture toughness as a function of mode mixity, the mixed mode criterion proposed by Benzeggagh and Kenane [21] is adopted in analysis (B–K criterion)

$$\frac{G_{\mathrm{I}}+G_{\mathrm{II}}+G_{\mathrm{III}}}{G_{\mathrm{IC}}+(G_{\mathrm{IIC}}-G_{\mathrm{IC}})((G_{\mathrm{I}}+G_{\mathrm{II}})/(G_{\mathrm{I}}+G_{\mathrm{II}}+G_{\mathrm{III}}))^{\eta}}=1 \tag{9}$$

where G_i and G_{ic} (i = I, II, III) are SERR and interface fracture toughness components, respectively, and η is a parameter obtained by fitting the experimental data.

In this paper, the commercial FEM code ABAQUS [22] is adopted to carry out numerical calculations. Fig. 5 shows a typical finite element model for the tri-layer TBC system. Four-node plane strain elements are selected for all the three layers. Nodes are allocated in pair at the left and right boundaries of the model. Regarding the periodicity of the problem, these nodes have been constrained under periodic conditions, where the opposite left and right edges of the representative cell model should remain parallel in a tangential sense [23,24]. To analyze the interfacial fracture behavior, cohesive elements are inserted between the ceramic top coat and the bond coat, as shown in Fig. 5, and fine meshes are used around the interface to improve the accuracy of the numerical results. The material parameters [25] of the cohesive elements are listed in Table 1. Two-dimensional forms of Eqs. (8) and (9) are used to describe the initiation and propagation of the cohesive element. Herein, each layer is taken to be homogeneous, isotropic and linear elastic materials. The material

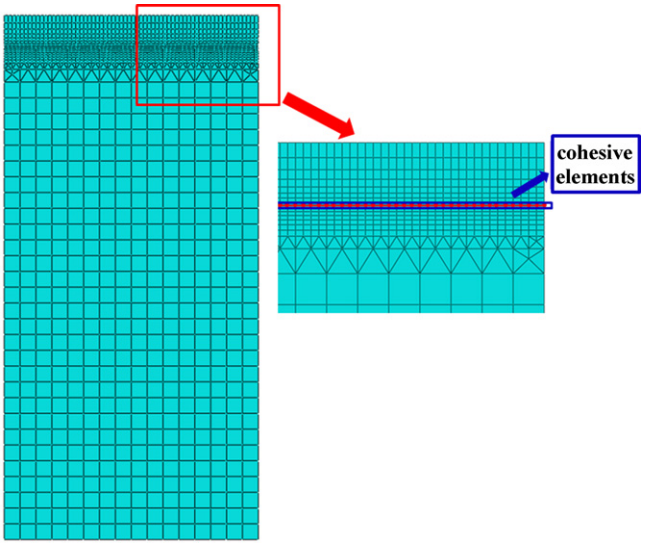

Fig. 5. An example finite element model with cohesive elements along the interface between the top coat and the bond coat.

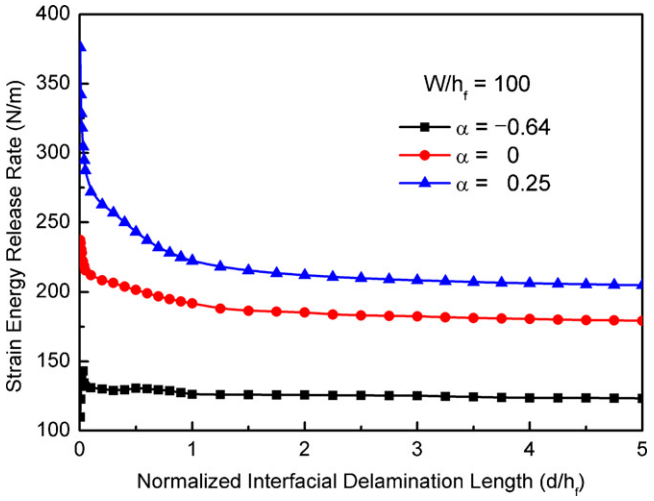

Fig. 6. The interface crack tip strain energy release rate as a function of normalized interfacial delamination length d/h_f for different material mismatch parameter α.

properties are E_f = 48 GPa, E_{BC} = 200 GPa, E_S = 211 GPa, ν_f = 0.1 and $\nu_s = \nu_{BC}$ = 0.3, where the subscripts f, s and BC represent film, substrate and bond coat, respectively. Different mismatched material properties are obtained by changing the Young's modulus and the Poisson's ratio of the coating.

3. Results and discussions

3.1. Effect of material mismatch on the driving force of interface crack

The effects of elastic mismatch parameter α defined by Eq. (1) on SERR is shown in Fig. 6, where the evolution of SERR is a function of interfacial delamination length for three cases of material combinations. In the case of $\alpha < 0$, i.e. the film is relative compliant as most of the cases in TBC system, the SERR increases to the maximum value and then decreases to a steady stage as interface crack propagates. The maximum value of crack driving force for $\alpha < 0$ is an important parameter for determining the emanation of interfacial delamination. In this case, i.e. $\alpha < 0$, the crack driving force approaches to zero as $d \to 0$, which implies that the crack driving force will vanish at the root of the surface crack for relative compliant film deposited on stiffer substrate. In comparison, in the case of $\alpha > 0$, the SERR becomes unbounded as $d \to 0$. As expected, in the case of no elastic mismatch between the top and the bond coats, i.e. $\alpha = 0$, the SERR lies between those of $\alpha < 0$ and $\alpha > 0$. Finally, in each case once the crack length is sufficiently long, the crack driving force becomes independent of the interfacial delamination length. In other words, a steady state exists for interfacial delamination. Interestingly, although the geometry is different, the present data have similar trend with those described by Mei et al. [15].

The mode mixity ψ is an important parameter to describe the combination of interface SERR or SIF components. Fig. 7 shows the variation of ψ as a function of normalized length of interfacial debonding for different material mismatch parameter α. During the process of initiation and propagation of interfacial delamination from the root of surface crack, there is a dramatic change of mode mixity ψ. The dependence of ψ on the elastic mismatch of materials is confined within a relative small range of interfacial delamination length. For all the possible material combinations, the effect of ψ is within the scale of film thickness, as shown in Fig. 7. It should be noted that for the positive material mismatch parameter ($\alpha > 0$), ψ asymptotically approaches the case of $\alpha = 0$. On the other hand, if

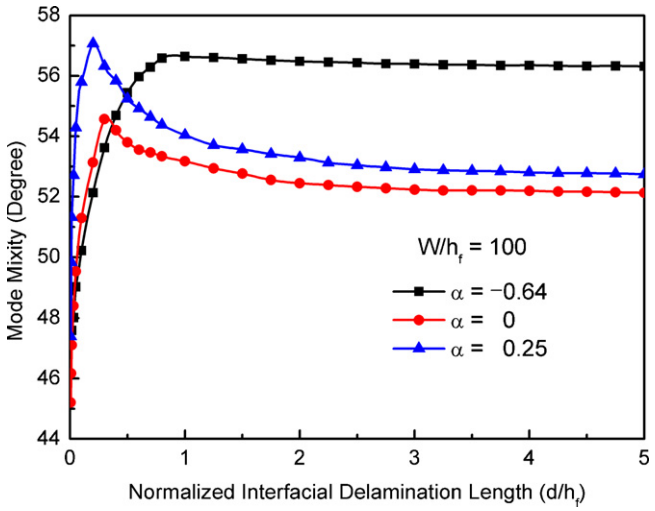

Fig. 7. Mode mixity vs normalized interfacial delamination length d/h_f for different material mismatch parameter α.

$\alpha < 0$, then ψ asymptotically approaches a steady value that is much higher than those of zero elastic mismatch ($\alpha = 0$).

The real and imaginary parts K_1 and K_2 of complex SIF play the same role as their counterparts in homogeneous isotropic materials. Therefore, the amplitude of the singularity of normal stress ahead of the interface crack tip is represented by the mode I SIF component K_1, which can be used to describe the normal separation of the interface. Similarly, the relative shear separation is governed by the mode II SIF component K_2. Also, the ratio of K_2 to K_1 based on a reference length is essential to obtain mode mixity ψ defined by Eq. (7). So, the distributions of normalized SIF components as a function of normalized length of interfacial delamination are shown in Fig. 8 for different material combinations. For an interfacial crack between two dissimilar isotropic materials, K_1 and K_2 are no longer the pure Mode I and Mode II SIF components. They are simply the real and imaginary parts of a complex SIF. In this case, an interaction integral method, as described in detail in "Stress intensity factor extraction," Section 2.16.2 of the Abaqus Theory Manual [22], can be used to compute the SIF components directly for a crack under mixed-mode loading. Herein, the SIF components K_1 and K_2 are normalized by $\sigma_f \sqrt{h_f}$ with σ_f being the stress in the film. It is seen that a relatively stiff film will develop much high normal stress and the corresponding SIF components are larger. On the contrary, a relatively compliant film experiences lower shear stress during the process of damage initiation and approaches a higher stable stage when the delamination is sufficiently long. The contact of the interface crack surfaces is more likely happened in this case.

3.2. *Effect of surface crack spacing on the driving force of interface crack*

The effect of periodic channeling crack spacing on the interfacial fracture of TBC system is discussed in this section, which is interesting and may offer the potential to improve the durability of TBC system by modifying the surface crack morphology.

For the interface crack emanated from the root of one dominate surface crack, it is found that if the interfacial delamination is long enough then SERR becomes independent of the delamination length. In other words, a steady state exists and the energy released per unit advance of crack no longer depends on the length of interfacial delamination. The steady state concept plays an important role in studying the stable and/or unstable propagation of interfacial delamination. The variations of interface crack driving force as a function of delamination length are shown in Fig. 9 for

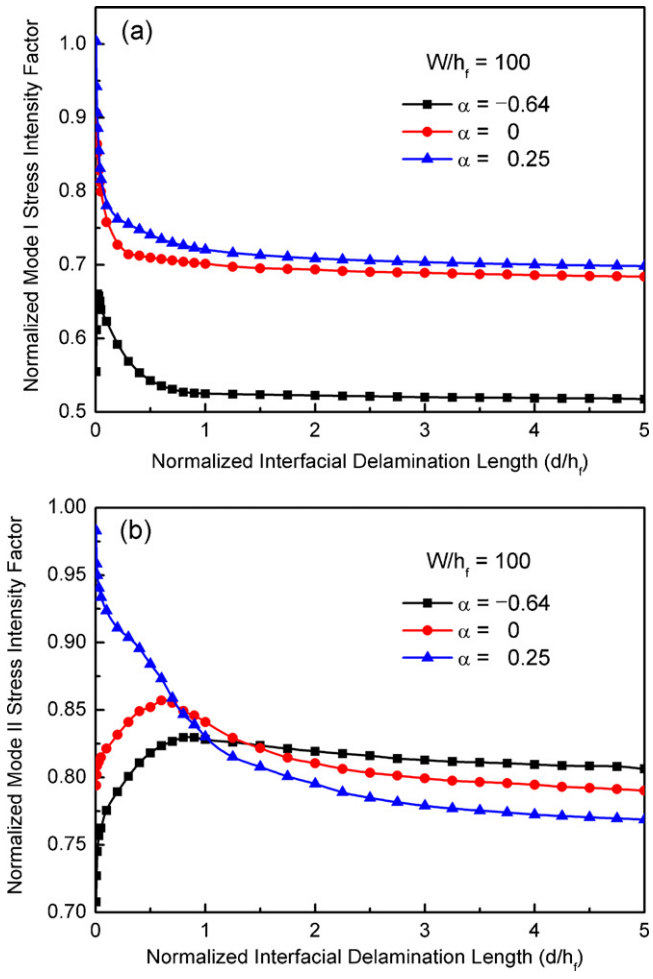

Fig. 8. Normalized stress intensity factor components vs normalized interface crack length d/h_f for different material mismatch parameter α. (a) K_1 for mode I crack and (b) K_2 for mode II crack.

different normalized surface crack spacing. Apparently, SERR for interfacial crack strongly depends on the surface crack spacing. Considering the curve in Fig. 9 for $w/h_f = 10$, SERR decreases sharply with increasing the length of interfacial delamination, which means

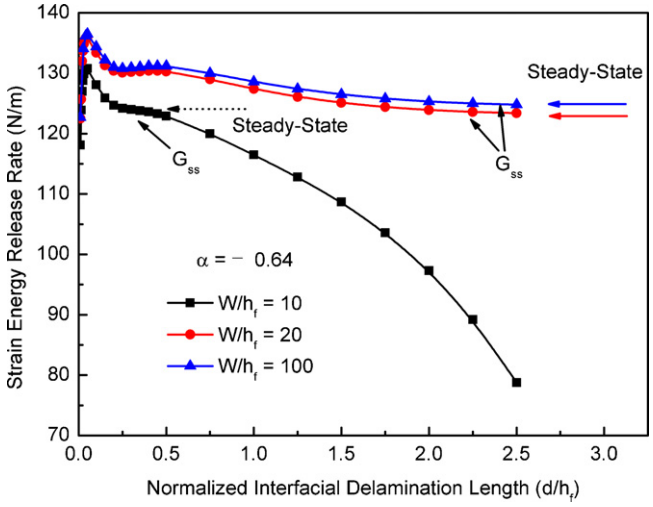

Fig. 9. The strain energy release rate as a function of normalized interfacial delamination length for different normalized surface crack spacings W/h_f. G_{SS} is the steady state strain energy release rate.

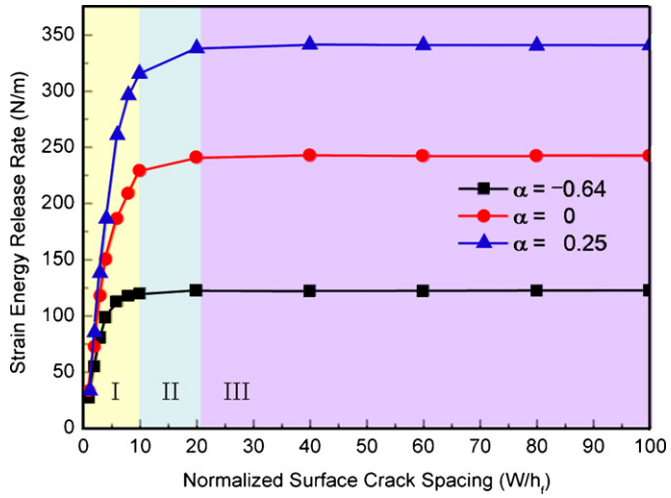

Fig. 10. The steady state strain energy release rate as a function of normalized surface crack spacing W/h_f for different elastic mismatch parameters.

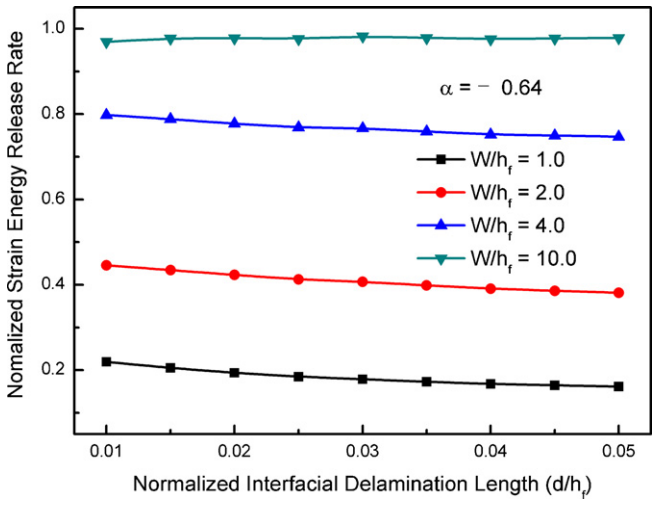

Fig. 12. The variation of the normalized strain energy release rate with short interfacial delamination for different normalized surface crack spacings W/h_f.

that the delamination will be arrested in this case. In contrast, considering the curves in Fig. 9 for $w/h_f = 20$ and 100, a steady sate is reached and the critical delamination length for the steady state crack propagation is only about two times the film thickness. Although there is essentially no steady state in the case of small surface crack spacing, for ease of comparison, an effective steady state SERR, G_{SS}, for high surface crack density situation is defined by the nearly steady state just before the dramatically decreases of the SERR for high surface crack density situations. Firstly, the effective steady state SERR for $w/h_f = 10$ is smaller than those of $w/h_f = 20$ and 100. Secondly, for $w/h_f = 10$, the driving force monotonically decreases from the effective steady state SERR to a very small value as the interfacial delamination grows, which may lead to the interface crack arrested after certain amount of propagation. Finally, in the cases of $w/h_f = 20$ and $w/h_f = 100$, both the evolution and the final steady state of SERR are comparable. In other words, the differences are insignificant for these two cases. Therefore, the surface crack spacing must be less than twenty times the film thickness in order to yield a significant effect on crack driving force of interracial delamination.

Curves of the steady state SERR G_{SS} as a function of normalized surface crack spacing W/h_f are shown in Fig. 10 for different material mismatch parameter α and in Fig. 11 for various normalized length of interfacial delamination d/h_f. As expected for small

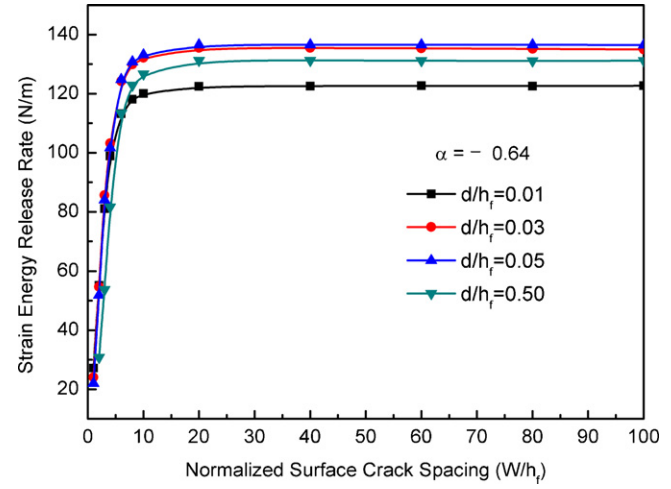

Fig. 11. The strain energy release rate as a function of surface crack spacing W/h_f for various normalized interfacial delamination lengths d/h_f.

interfacial delamination, surface crack spacing has a notable effect on the crack driving force. As $d \to 0$, the steady state SERR decreases dramatically for each case as the surface crack spacing W decreases (Fig. 10). In comparison, if the surface crack spacing is sufficiently large, then the crack driving force reaches a stable stage and the difference become indistinguishable for a given material mismatch. In other words, the results will finally merge with those of only one dominate surface crack in the film.

It is seen from Figs. 10 and 11 that there are three different regions identified to separate the degree of surface crack spacing effect on the interface crack. In Region I, surface crack spacing has a significant effect on the driving force of interface crack. In this case, the initiation of interfacial delamination and associated film debonding can be delayed or arrested. Region II is a transition zone, in which the effect of surface crack spacing gradually decreases as the interfacial delamination propagates. In Region III, a stable stage is reached, where the effect of surface crack spacing is insignificant and can be ignored. It is seen that the interface crack driving force becomes independent of surface crack spacing as the crack spacing is large enough, approximately twenty times the film thickness, i.e. $w/h_f \geq 20$ for the present problem.

The variations of normalized SERR as a function of normalized delamination length d/h_f are shown in Fig. 12 for different normalized surface crack spacings W/h_f, in which the reference value of SERR is that of only one surface crack in the coating (i.e., $W/h_f \to \infty$) and the interfacial delamination length is small enough to emphasize the markedly dependence of short interface crack on surface crack spacing. It has been pointed out that the propagation of short interface crack will markedly change the crack tip stress and displacement fields, see Figs. 6 and 8 for detail. However, the effect of surface crack spacing on the driving force of interfacial delamination is much more significant than that of interface crack length, as shown in Fig. 12. For a given surface crack spacing, the effect of interfacial delamination length can be considered as negligible since the SERR decreases dramatically as W/h_f decreases, even for very short interfacial delamination. Take $W/h_f = 1$ as an example, SERR approximately reduces to 20% the values for $W/h_f = 10$. Note that all the normalized surface crack spacings in Fig. 12 are smaller than the size of transition zone size.

3.3. *Effect of surface crack spacing on interfacial delamination behavior*

The aforementioned numerical results show that the surface crack spacing has a significant effect on the driving force of

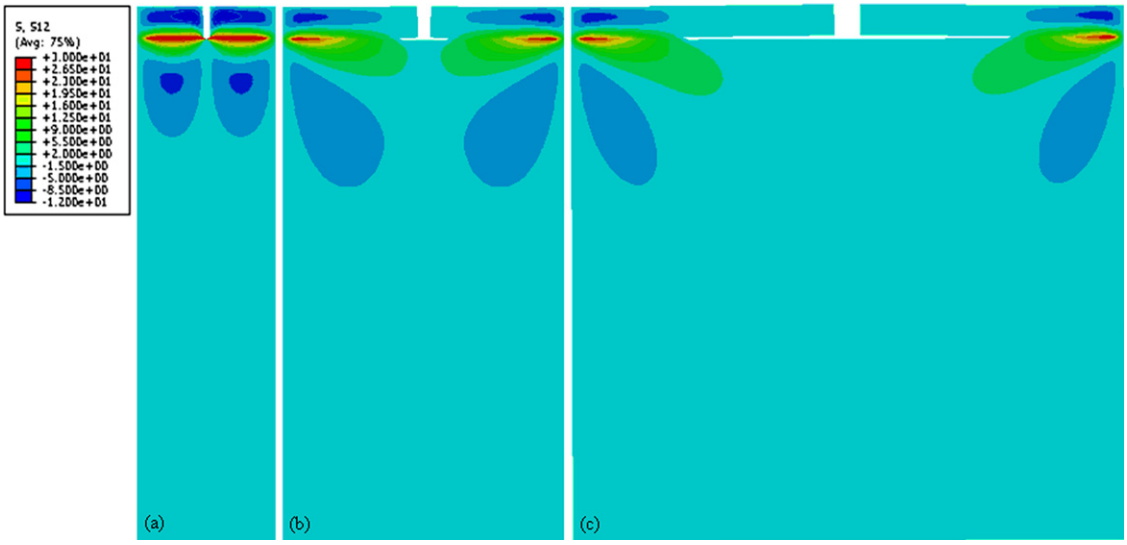

Fig. 13. Interfacial delamination behaviors for different cases of normalized surface crack spacings: (a) $W/h_f = 10$, (b) $W/h_f = 20$, and (c) $W/h_f = 30$.

interfacial delamination, which may determine whether or not the surface cracks turn into the interface between the top and bond coats. If interfacial delamination does initiate from the root of surface crack, it believes that the damage evolution will also be severely affected by the surface crack spacing. The interfacial fracture behavior is therefore considered in this section. Three typical normalized surface crack spacing $W/h_f = 10$, 20 and 30 (different regions shown in Fig. 10) are selected for the case of a specific minus material mismatch ($\alpha = -0.64$). Other parameters are the same as above.

For the case of $W/h_f = 10$ (Region I in Fig. 10), the driving force of interface crack is much smaller than that of the stable case. Consequently, no interfacial delamination occurs if the SERR is less than the interfacial fracture toughness. In this case, W/h_f is much smaller than the critical value of normalized surface crack spacing and no concomitant interfacial delamination occurs, as shown in Fig. 13(a). In the case of $W/h_f = 20$ (the transition zone II in Fig. 10), interfacial delamination emanates from the root of surface crack, however, arrests after small distance of propagation, as shown in Fig. 13(b). For the case of $W/h_f = 30$ (Region III in Fig. 10), the driving force of interface crack is stable and approaches the results of only one surface crack in the film. Numerical results indicate that the effect of adjacent surface cracks can be ignored in this case. Apparently, the driving force for interfacial delamination is significantly higher than that of high surface crack density. So, the interfacial delamination initiates and propagates until a catastrophic failure occurs with increasing external loads, as shown in Fig. 13(c). In this case, most of the interface cohesive elements are damaged and large areas of debonding may occur. These results are important. It means that the possibilities of concomitant interfacial delamination and unstable interface crack propagation may be reduced by increasing the density of surface cracks to some extent, which can be adopted to delay the coatings debonding in TBC system.

4. Conclusions

The effect of periodic surface crack spacing on the interfacial fracture is interesting and offers the potential for improving the durability of thermal barrier coating (TBC) system by modifying the surface crack morphology. A finite element model incorporating the cohesive element zone method is adopted to study the initiation and propagation of interfacial delamination emanating from the root of surface crack. It is concluded that interfacial delamination can easily be initiated between a stiffer top coat and a relatively compliant bond coat. Normalized critical surface crack spacing is an important parameter to indicate the separatrix whether the interactive behavior of multiple surface cracks and interfacial delamination should be taken into account or not. The effect of multiple surface cracks on the interface delamination is significant as the inter-space between the surface cracks is less the critical spacing, while the interactive behavior is insignificant and can be neglected as crack space is greater that the critical spacing. The critical surface crack spacing is about twenty times of the coating thickness, which agreed well with our experimental observation (Fig. 1). In the case of high surface crack density, surface crack may propagate without interfacial delamination. In other words, the initiation of interfacial delamination may be arrested when surface crack spacing is smaller than the critical value. In case of a weak interface, however, interfacial delamination can occur concomitantly with low density of surface cracks. Based on these results, we can conclude that an appropriately high surface crack density can enhance the durability of TBC system by reducing the possibility of coating debonding.

Acknowledgements

National Natural Science Foundation of China (11002104 and 11021202), NSF of Shaanxi Province (2011JQ1019) and Fundamental Research Funds for Central Universities (xjj2011053, GCKY1004).

References

[1] M.S. Hu, A.G. Evans, Acta Metall. 37 (1989) 917–925.
[2] T.Q. Lu, W.X. Zhang, T.J. Wang, Int. J. Eng. Sci. 49 (2011) 967–975.
[3] T.J. Wang, Eng. Fract. Mech. 44 (1993) 971–980.
[4] F. Erdogan, J. Appl. Mech. Trans. ASME 52 (1985) 823–828.
[5] G.W. Schulze, F. Erdogan, Int. J. Solids Struct. 35 (1998) 3615–3634.
[6] K. Kokini, B.D. Choules, T.A. Taylor, Mater. Sci. Eng. A 299 (2001) 296–304.
[7] X.L. Fan, W.X. Zhang, T.J. Wang, G.W. Liu, J.H. Zhang, Appl. Surf. Sci. 257 (2011) 6718–6724.
[8] W.X. Zhang, X.L. Fan, T.J. Wang, Appl. Surf. Sci. 258 (2011) 811–817.
[9] A.A. Rizk, Int. J. Solids Struct. 41 (2004) 4685–4696.
[10] M.D. Thouless, Z. Li, N.J. Douville, S. Takayama, J. Mech. Phys. Solids 59 (2011) 1927–1937.

[11] M.C. Lu, F. Erdogan, Eng. Fract. Mech. 18 (1983) 491–506.
[12] B. Zhou, K. Kokini, Mater. Sci. Eng. A 348 (2003) 271–279.
[13] B. Zhou, K. Kokini, Acta Mater. 52 (2004) 4189–4197.
[14] C.W. Wu, G.N. Chen, K. Zhang, G.X. Luo, N.G. Liang, Surf. Coat. Technol. 201 (2006) 287–291.
[15] H.X. Mei, Y.Y. Pang, R. Huang, Int. J. Fract. 148 (2007) 331–342.
[16] J.W. Hutchinson, Z. Suo, Adv. Appl. Mech. 29 (1992) 63–191.
[17] M.Y. He, J.W. Hutchinson, Int. J. Solids Struct. 25 (1989) 1053–1067.
[18] D.S. Dugdale, J. Mech. Phys. Solids 8 (1960) 100–104.
[19] A. Needleman, J. Appl. Mech. Trans. ASME 54 (1987) 525–531.
[20] L. Ye, Compos. Sci. Technol. 33 (1988) 257–277.
[21] M.L. Benzeggagh, M. Kenane, Compos. Sci. Technol. 56 (1996) 439–449.
[22] ABAQUS User's Manual, Dassault Systèmes Simulia Corporation, 2009.
[23] W.X. Zhang, T.J. Wang, L.X. Li, Comput. Mater. Sci. 39 (2007) 684–696.
[24] Z.M. Xu, W.X. Zhang, T.J. Wang, Int. J. Appl. Mech. 2 (2010) 489–513.
[25] R.G. Hutchinson, J.W. Hutchinson, J. Am. Ceram. Soc. 94 (2011) S85–S95.